Journal of Alloys and Compounds 963 (2023) 171246

Contents lists available at ScienceDirect

Journal of Alloys and Compounds

journal homepage: www.elsevier.com/locate/jalcom

Harnessing the potential of Dion-Jacobson perovskite solar cells: Insights from SCAPS simulation techniques

Mustafa K.A. Mohammed [a,*,1], Ali K. Al-Mousoi [b,1], Anjan Kumar [c], Michael M. Sabugaa [d], Ramanjaneyulu Seemaladinne [e], Rahul Pandey [f], Jaya Madan [f], M. Khalid Hossain [g], Burragoni Sravanthi Goud [h,1], Abdullah A. Al-Kahtani [i]

[a] University of Warith Al-Anbiyaa, 56001 Karbala, Iraq
[b] Electrical Engineering Department, College of Engineering, Al-Iraqia University, Baghdad 10011, Iraq
[c] Department of Electronics and Communication Engineering, GLA University, Mathura-281406, India
[d] Department of Electronics Engineering, Agusan del Sur State College of Agriculture and Technology, Philippines
[e] Department of Chemistry and Biochemistry, Lamar University, Beaumont, TX 77710, USA
[f] VLSI Centre of Excellence, Chitkara University Institute of Engineering and Technology, Chitkara University, 140417 Rajpura, Punjab, India
[g] Institute of Electronics, Atomic Energy Research Establishment, Bangladesh Atomic Energy Commission, Dhaka 1349, Bangladesh
[h] Department of Chemical Engineering, Yeungnam University, 214-1, Daehak-ro 280, Gyeongsan 712–749, Gyeongbuk-do, Republic of Korea
[i] Department of Chemistry, College of Science, King Saud University, P. O. Box 2455, Riyadh 11451, Saudi Arabia

ARTICLE INFO

Keywords:
SCAPS
Dion-Jacobson
Solar cells
Efficiency
Perovskite

ABSTRACT

Although perovskite solar cells (PSCs) have shown considerable advancement in recent years, their extensive usage is hindered by the major challenge of ensuring long-term stability. However, the enhanced stability of 2D-structure Dion-Jacobson (DJ) phase halide perovskites makes them a promising alternative to the traditional 3D perovskites, suggesting potential for broader application. In this numerical simulation, bulky organic ammonium spacer pentamethylenediamine (PeDA) was incorporated into DJ perovskite films with four different layer numbers (n = 3, 4, 5, and 6), which correspond to $PeDAMA_2Pb_3I_{10}$, $PeDAMA_3Pb_4I_{13}$, $PeDAMA_4Pb_5I_{16}$, and $PeDAMA_5Pb_6I_{19}$, respectively. Various parameters were adjusted to assess their impact on device performance. A current density–voltage (J-V) characterization was conducted for each value of n to compare their efficiencies. The number of layers was found to significantly influence efficiency, with the highest performance achieved at n = 6, resulting in an open-circuit voltage (V_{OC}) of 1.27 V, a short-circuit current density (J_{SC}) of 22.83 mA/cm^2, a power conversion efficiency (PCE) of 21.17%, and a fill factor (FF) of 72.72%. These results demonstrate the potential of DJ perovskite solar cells with PeDA spacers as stable and efficient alternatives for photovoltaic applications.

1. Introduction

These cells have gained significant attention in recent years due to their high efficiency, low cost, and potential for scalability. One of the main advantages of perovskite solar cells is their high efficiency [1–5]. In just a few years, scientists have increased the efficiency of PSCs from 4% to over 25%, which is almost identical to the performance of conventional silicon solar cells [6–9]. The dramatic rise in efficiency is the result of a number of aspects like enhancements in the perovskite substances utilized, an improved comprehension of the fundamental physics of the cells, and progress in the manufacturing process [10–15].

Dion-Jacobson (DJ) PSCs have been identified as a potential photovoltaic technology of the next generation, demonstrating outstanding prospects for highly efficient and economical solar energy production [16–18]. The distinct stacked structure of DJ perovskites, which involves consecutive inorganic and organic layers, provides superior optoelectronic characteristics and improved durability, which renders them ideal choices for application in solar cells [19,20]. Basically, 2D layered perovskites are produced by dividing their dense organic ammonium 3D counterparts into one or more layer segments in a

* Corresponding author.
E-mail address: mustafa_kareem97@yahoo.com (M.K.A. Mohammed).
[1] These authors contributed equally.

https://doi.org/10.1016/j.jallcom.2023.171246
Received 22 March 2023; Received in revised form 13 June 2023; Accepted 3 July 2023
Available online 4 July 2023

Table 1
The input parameters of FTO/PCBM/DJ Perovskite/NiOx /Au 2D perovskite solar cells [16].

Device Layer Properties	Device Layers						
	Unit	PCBM	$PeDAMA_2Pb_3I_{10}$	$PeDAMA_3Pb_4I_{13}$	$PeDAMA_4Pb_5I_{16}$	$PeDAMA_5Pb_6I_{19}$	NiO_x
Thickness	nm	50	200–1000	200–1000	200–1000	200–1000	100
Energy Gap	eV	2	1.83	1.76	1.65	1.6	3.5
Electron Affinity Energy	eV	4	3.15	3.28	3.64	3.98	1.8
Electron Mobility	$cm^2/V.s$	0.02	1.4	1.4	1.4	1.4	12
Hole Mobility	$cm^2/V.s$	0.02	0.3	0.3	0.3	0.3	2.8
Acceptor Concentration	$1/cm^3$	0	0	0	0	0	3×10^{18}
Donor Concentration	$1/cm^3$	1×10^{16}	0	0	0	0	0
CB effective density of states	$1/cm^3$	1.17×10^{19}	7.5×10^{17}	7.5×10^{17}	7.5×10^{17}	7.5×10^{17}	2.8×10^{19}
VB effective density of states	$1/cm^3$	1.12×10^{19}	1.8×10^{18}	1.8×10^{18}	1.8×10^{18}	1.8×10^{18}	1×10^{19}
Dielectric Permittivity	-	3.9	25	25	25	25	10.7
Defect type	-	Neutral	Neutral	Neutral	Neutral	Neutral	Neutral
Capture cross section of electrons	cm^2	1×10^{-15}	1×10^{-15}	1×10^{-15}	1×10^{-15}	1×10^{-15}	1×10^{-15}
Capture cross section of holes	cm^2	1×10^{-15}	1×10^{-15}	1×10^{-15}	1×10^{-15}	1×10^{-15}	1×10^{-15}
Total defect density	$1/cm^3$	1×10^{16}	2.5×10^{14}	2.5×10^{14}	2.5×10^{14}	2.5×10^{14}	1×10^{15}

Table 2
Interface parameters of FTO/PCBM/DJ Perovskite /NiO_x/Au PSCs [37].

Parameters/Interfaces	PCBM/DJ Perovskite	DJ Perovskite/NiO_x
Type of Defect Present	neutral	neutral
Cross-Section for Electron Capture (cm^2)	1×10^{-15}	1×10^{-15}
Cross-Section for Hole Capture (cm^2)	1×10^{-15}	1×10^{-15}
Distribution of Energies	single	single
Reference for Energy Level of Defect (E_t)	Above the highest E_v	Above the highest E_v
Energy Measured with Respect to Reference (eV)	0.600	0.600
Total Density of Defects ($1/cm^2$)	1×10^{10}	1×10^{10}

specific direction [14–16]. The 2D perovskite phases illustrate a wide variety of crystalline alignments when compared to the planes of the 3D parents construction. These directions are defined by the large spacer cations that split the octahedra and encompass the 100-, 110-, and 111-oriented configurations [21]. These orientations are defined by the large spacer cations that separate the octahedra, and include the ⟨100⟩-oriented, ⟨110⟩-oriented, and ⟨111⟩-oriented structures [22]. The 100-oriented 2D perovskites are the orientation most frequently researched and contemplated. These substances can be divided into three categories: the Ruddlesden-Popper (RP) phase [19], the Dion-Jacobson (DJ) phase, and the alternating cations in the interlayer space (ACI) phase. The chemical rules for each of these phases are A′2An− 1MnX3n+ 1, A′An− 1MnX3n+ 1, and A′AnMnX3n+ 1, respectively, where A′ refers to the long chain spacer cation, A represents the organic cation, X symbolizes the halide anion, M indicates a divalent metal, and n is an integer that represents the number of [PbX6]4– octahedral sheets compacted between two layers of A′ spacer cations [23,24].

In 2019, Zheng and colleagues conducted a study to investigate the impact of quantum well (QW) barrier thickness on the orientation and uniformity of Dion-Jacobson (DJ) phase perovskite films. Their results demonstrated that by controlling the thickness of the QW barrier, they could achieve better orientation and more uniform distribution of DJ phase perovskites, which could lead to significant improvements in the performance of perovskite-based optoelectronic devices. Specifically, the authors found that DJ phase perovskite photovoltaic devices fabricated using PDA and BDA exhibited significantly higher power conversion efficiencies (PCEs) of 14.16% and 16.38%, respectively, compared to PCEs of 12.95% and 10.55% observed for PeDA and HDA analogs [16]. These results indicate that modulating the thickness of the QW barrier may offer an attractive option for improving the efficiency of DJ phase PSCs [13]. Zhang et al. present their research aimed at boosting the performance of DJ PSCs through the use of Bromine-rich cations for anion modification in 2022. The researchers designed several kinds of DJ perovskite via replacing the anion Chlorine with Bromine and revealed that the corresponding Br-rich DJ perovskites had superior absorbance of light, drastically decreased trapping magnitude, and enhanced charge mobility relative to the Cl-rich DJ perovskites. The modified Br-rich DJ PSCs gained a PCE of 17,1%, which is greater than the 15.5% PCE reached by the optimized Cl-rich DJ PSCs. The investigation demonstrates that integrating Br-rich cations into anion architecture could be a successful strategy for enhancing the performance of DJ PSCs [22].

In this study, we use SCAPS-1d to model and simulate DJ PSCs, concentrating on the resultant impact of important parameters that involve perovskite layer dimension, series and shunt resistance. We examine the relationship among these factors and the general functionality of the device in an effort to identify the ideal conditions for attaining the greatest achievable PCE. In addition, we investigate fresh ideas for minimizing the challenges related to DJ PSCs, such as shunt and series resistance.

By means of SCAPS-1d modeling, we present an in-depth understanding of the principles governing the performance of DJ PSCs as well as viable options for maximizing their performance. Our results provide significant guidance for the development and manufacturing of highly efficient DJ PSCs, which will benefit the progress of this newly developed solar energy technology and the possible effect it will have on the solar energy field. In addition, we conduct important examination to ascertain the validity of the results we obtained and offer suggestions for future studies. We also compare the simulated performance of DJ perovskite solar cells with experimental results reported in the literature, validating the accuracy and reliability of our simulations. In conclusion, our study serves as a valuable reference for researchers and engineers working on DJ perovskite solar cells, offering a solid foundation for further advancements.

2. 2D-DJ perovskite solar cell simulation

Numerical modeling of solar cell devices allows for a comprehensive understanding of device dynamics without the need for actual manufacturing. This enables a high-level overview of device functionality. For this simulation study, the one-dimensional SCAPS (version

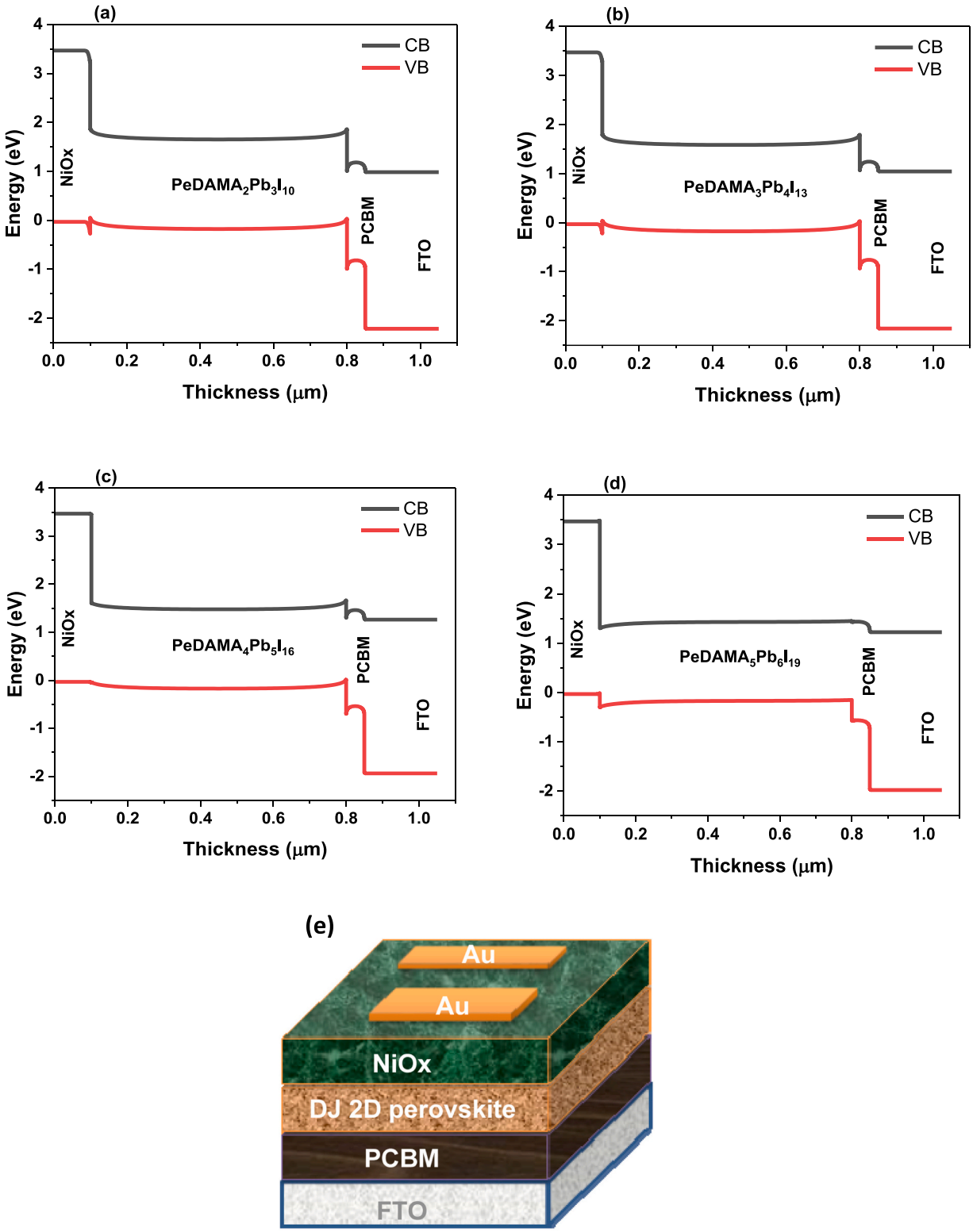

Fig. 1. The band alignment diagram of (a) $PeDAMA_2Pb_3I_{10}$, (b) $PeDAMA_3Pb_4I_{13}$, (c) $PeDAMA_4Pb_5I_{16}$ and (d) $PeDAMA_5Pb_6I_{19}$. (e) Solar cell structure utilized in this simulation.

3.3.07) was utilized. SCAPS is an open-source program created by researchers at the University of Gent in Belgium in 2000 that can be downloaded at any time [25]. It assists in modeling planar and graded PV structures up to seven components and provides additional functionality for calculating band alignment graphs, current-voltage (*J-V*) behavior, quantum efficiency (QE), recombination and generation currents, and other essential PV characteristics [26,27]. The SCAPS-1D relies primarily on Poisson's formula and the continuity laws for electrons and holes to perform calculations. The Poisson equation, continuity equation for the hole, and continuity equation for the electron are used for modeling [28–31].

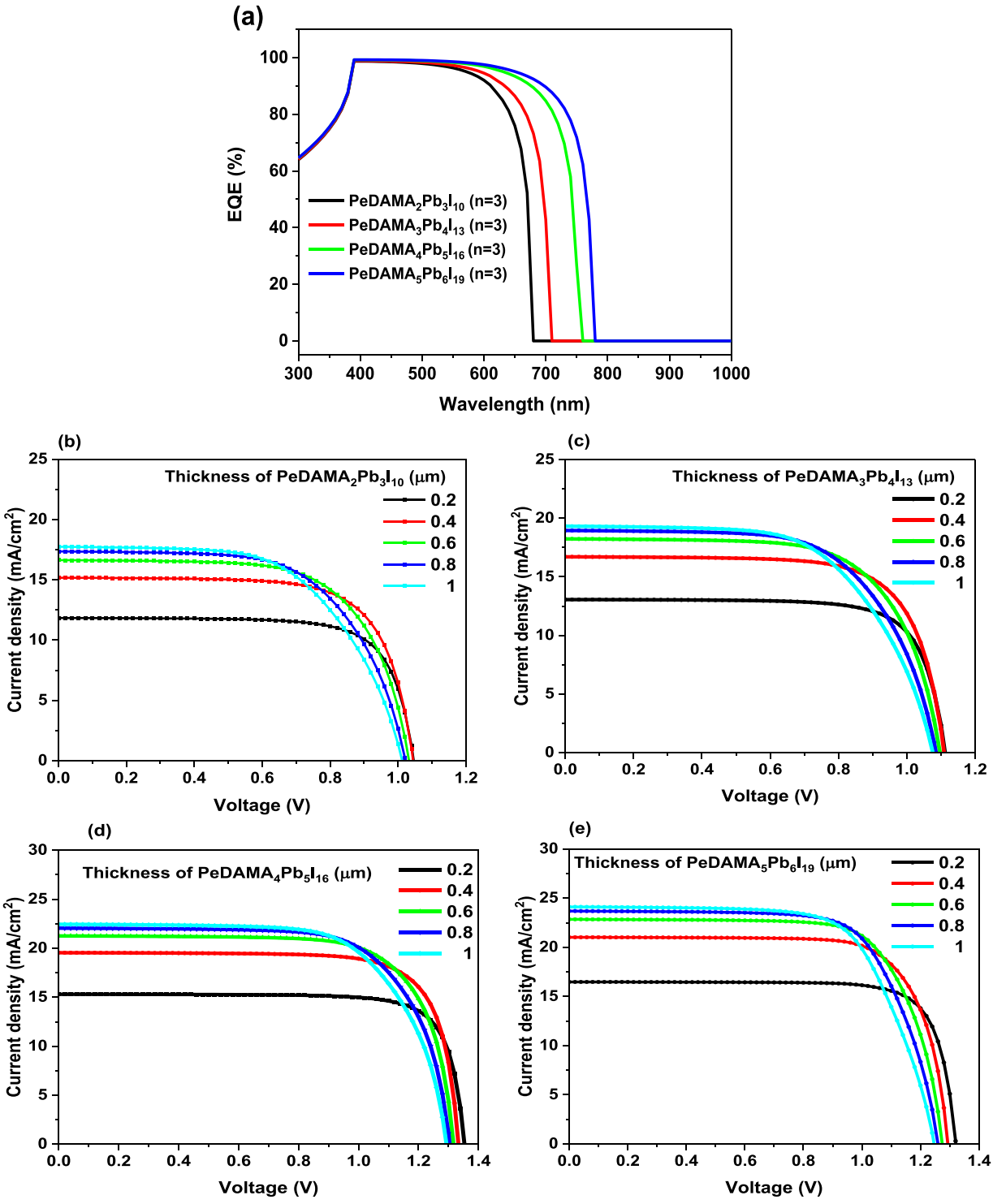

Fig. 2. (a) EQE of devices with various DJ perovskite. (b, c, d and e) are the J-V curve with different thickness of $PeDAMA_2Pb_3I_{10}$ ($n = 3$), $PeDAMA_3$ Pb_4I_{13} ($n = 4$), $PeDAMA_4Pb_5I_{16}$ ($n = 5$) and $PeDAMA_5Pb_6I_{19}$ ($n = 6$) with different based PSCs respectively.

$$\text{Poisson equation}: -\frac{\partial}{\partial x}\left(\varepsilon(x)\frac{\partial V}{\partial x}\right) = q[p(x)n(x) + N_D^+(x) - N_A^-(x) + p_t(x) - n_t(x)] \quad (1)$$

$$\text{Continuity equation for the hole}: \frac{\partial p}{\partial t} = \frac{1}{q}\frac{\partial J_p}{\partial x} + G_p - R_p \quad (2)$$

$$\text{Continuity equation for the electron}: \frac{\partial n}{\partial t} = \frac{1}{q}\frac{\partial J_n}{\partial x} + G_n - R_n \quad (3)$$

In the equation set, q represents the charge, V represents the potential, $p(x)$ denotes the concentration of free holes, $n(x)$ represents the concentration of free electrons, ε represents the dielectric permittivity, $N_D^+(x)$ represents the donor density, $N_A^-(x)$ denotes the acceptor density, $p_t(x)$ represents the hole trap concentration, $n_t(x)$ represents the trap

Table 3
Parameters of FTO/PCBM/DJ Perovskite /NiOx/Au PSCs with different perovskite thicknesses for various DJ perovskite layers.

Perovskite	Thickness (μm)	V_{OC} (V)	J_{SC} (mA/cm^2)	FF (%)	PCE (%)
$PeDAMA_2Pb_3I_{10}$	0.2	1.046	11.832	74.050	9.171
	0.4	1.044	15.169	71.018	11.258
	0.6	1.032	16.628	66.233	11.375
	0.8	1.021	17.347	62.374	11.056
	1.0	1.012	17.736	59.522	10.689
$PeDAMA_3Pb_4I_{13}$	0.2	1.112	13.054	75.203	10.920
	0.4	1.109	16.702	71.971	13.340
	0.6	1.097	18.231	67.264	13.456
	0.8	1.085	18.950	63.603	13.089
	1.0	1.076	19.316	60.919	12.667
$PeDAMA_4Pb_5I_{16}$	0.2	1.353	15.300	79.296	16.425
	0.4	1.333	19.537	76.802	20.014
	0.6	1.317	21.252	72.868	20.396
	0.8	1.304	22.042	69.896	20.093
	1.0	1.293	22.443	67.695	19.654
$PeDAMA_5Pb_6I_{19}$	0.2	1.320	16.471	79.250	17.243
	0.4	1.294	21.014	74.994	20.392
	0.6	1.274	22.834	72.719	21.168
	0.8	1.259	23.674	70.544	21.039
	1.0	1.246	24.103	68.166	20.488

Table 4
Parameters of FTO/PCBM/DJ Perovskite/NiO/Au PSCs with different layer number.

Perovskite	V_{OC} (V)	J_{SC} (mA/cm^2)	FF (%)	PCE (%)
$PeDAMA_2Pb_3I_{10}$	1.027	17.04	64.15	11.23
$PeDAMA_3Pb_4I_{13}$	1.091	18.65	65.28	13.29
$PeDAMA_4Pb_5I_{16}$	1.31	21.71	71.26	20.27
$PeDAMA_5Pb_6I_{19}$	1.26	23.32	71.65	21.17

concentration of an electron, J_n represents the current density of an electron, J_p represents the current density of a hole, G_n represents the electron generation rate, G_p represents the holes generation rate, R_n denotes the recombination rate of electrons, and R_p denotes the recombination rate of holes [32–34].

In this simulation, a typical n-i-p PV architecture with $PeDAMA_{n-1}Pb_nI_{3n+1}$ (n is an integer) Dion-Jacobson (DJ) phase halide perovskite as the photoactive film, PCBM as the electron-transporting layer (ETL), NiO_x film as the hole-transporting layer (HTL), fluorine-containing SnO_2 (FTO) and gold (Au) as the front and back electrodes, respectively, was simulated. Table 1 and Table 2 summarize the fundamental device parameters of several materials utilized in this analysis that were acquired from the theoretical and experimental literature. The defects were set at 0.6 eV above the valence band with a particular energy of 0.1 eV, considering the Gaussian energy distribution and the capture cross-section of carriers of 10^{-15} cm^2 [35]. In the case of 2D DJ perovskites, they have a zero N_D and zero N_A because they do not contain any charged dopants. Instead, 2D DJ perovskites consist of alternating layers of inorganic and organic materials, with the inorganic layer forming the perovskite structure and the organic layer providing a barrier that prevents the diffusion of ions. The absence of charged dopants means that there are no extra charge carriers to contribute to the electronic conductivity of the material. The defect density of the active material was chosen to be 2.5×10^{14} cm^{-3} which corresponding to the electron diffusion length to be 1200 nm and hole diffusion length to be 560 nm [36]. The radiative recombination coefficient for perovskite was 2.3×10^{-9} cm^3/s, which was taken into consideration. The modeling analysis added imperfections at the HTL/perovskite and perovskite/ETL interfaces. The conventional AM 1.5 G spectrum and a temperature of 300 K were utilized for the computations. Overall, the SCAPS simulation provided a comprehensive understanding of the device dynamics and functionality of the DJ perovskite solar cell.

3. PCS's structural design and material characteristics

In this work, a proposed perovskite solar cell (PSC) structure, FTO/PCBM/DJ Perovskite/NiO_x/Au PSCs as shown in Fig. 1e, was investigated. The front transparent contact was made using an FTO layer on a glass substrate and a PCBM layer represented the ETL. DJ 2D Perovskite served as the absorbing layer, generating charge carriers via photon absorption. The HTL was made using NiO_x material. The suggested structure's energy band diagram indicated the conduction band of the perovskite layer was relatively small compared that of the ETL, with a minor mismatch between the conduction bands (CB) of DJ Perovskite and PCBM layer (Fig. 1a-d). This allowed electrons to easily pass from DJ Perovskite to FTO via PCBM. The mismatch in the conduction band tended to decrease with increasing n value, enabling more electrons to move freely and thus improving the performance of the solar cell. A large valance band offsetting existed between the absorber layer and the ETL, effectively sealing the positively charges (holes) at ETL material. The valence bands of the HTL material higher when compared to the absorber layer, with a significantly slight valence bands mismatch between these two layers. Moreover, the offset in the conduction band between the HTL material NiO_x and the absorbing material was very considerable, effectively prohibiting the electron from DJ Perovskite from approaching the Au layer. The proposed structure has the potential to enhance the performance of PSCs by improving the charge carrier generation and transport within the device.

4. Results and discussion

4.1. Optimization of Dion–Jacobson perovskite thickness

The efficiency of a solar cell is highly dependent on the thickness of the absorptive material, which is responsible for absorbing solar radiation and improving the *J-V* characteristic. In this work, the impact of the thickness of the DJ perovskite absorber material on the efficiency of the solar cells is evaluated. The material parameters are held constant, and the thickness of the DJ perovskite is varied to determine the optimal thickness. Fig. 2 presents the suggested parameters of the photovoltaic cell as a function of the DJ perovskite thickness. Fig. 2a depicts the EQE of the proposed PSC, and it is seen that the absorptive material's layer number (n) influences the EQE value. As the n value increases, so does the EQE value, as expected. Fig. 2b-e depicts the *J-V* curve of the PSC for various n values under 100 mW/cm^2 illumination (air mass AM 1.5 G). The shape of the *J-V* curve varies due to differences in the FF, V_{OC}, and J_{SC}, leading to changes in the PCE with varying thickness. The value of

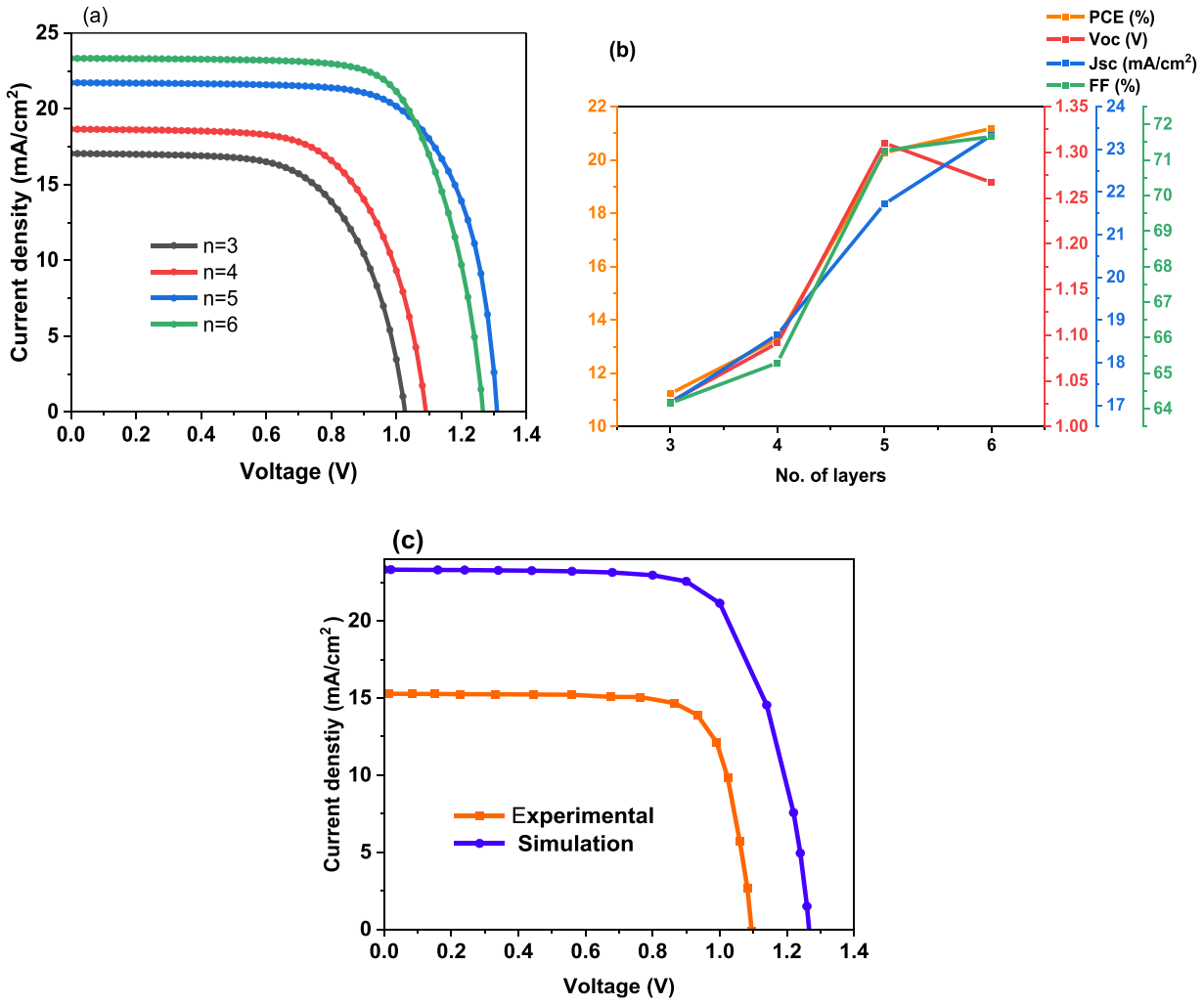

Fig. 3. (a) The *J-V* curves corresponding to the number of layer of the 2D DJ perovskite. (b) The device characteristics of the 2D DJ perovskite for each number of layers (c) The *J-V* curve estimated in experimental and our simulation.

V_{OC} is slightly altered when the thickness is varied, while the FF and J_{SC} are the most affected parameters by thickness variation. The DJ perovskite thickness of 0.6 μm leads to the best performance of the proposed solar cell, as it results in the overall changes in the solar cell parameters (see Table 3).

4.2. *Optimization of number of layers of the Dion-Jacobson perovskite*

The number of layers is a crucial parameter that significantly impacts the performance of Dion–Jacobson (DJ) perovskite solar cells. To optimize the number of layers, SCAPS simulations were utilized to systematically investigate the effect of different layer configurations on device performance. The results, presented in Table 4 and Fig. 3 a-b, demonstrate that increasing the number of layers leads to improvements in almost all device parameters. The highest-performing device, based on the proposed 2D perovskite, was achieved at n = 6. Furthermore, Fig. 3**c** compares the *J-V* curve of the experimental work, which achieved a PCE of 12.95%, with our simulated PCE of 21.17%. Because of the quantum confinement effect, the E_g of the perovskite may decrease as the number of layers in the two-dimensional perovskite rises. This phenomenon occurs when the material's sizes are less than the exciton Bohr radius, resulting in a rise in binding energy and a drop in effective E_g. A reduction in E_g can boost the V_{OC} of a PSC. This is due to the fact that the V_{OC} is proportional to the energy difference between the electron quasi-Fermi level in the ETL and the hole quasi-Fermi level in the HTL. A narrower E_g indicates that the perovskite can absorb photons with less energy, resulting in greater energy differences and an increased V_{OC} [38]. These simulation results highlight the superior performance achieved through the proposed device structure. This difference between the experimental and simulation results can be due to several factors. Firstly, there may be differences in the device fabrication process, which can lead to variations in the device's performance. The experimental PCE can be affected by various factors, such as the quality of the deposited layers, the uniformity of the device, and the contact resistance. Many different variables can cause in differences from anticipated results, eventually ending in reduced PCEs. The accuracy of the computational framework employed in the numerical calculation of the PCE may be questionable in terms of its ability to precisely replicate the physical characteristics of the experimental PSCs. The potential cause of this occurrence could be attributed to the presumptions incorporated in the simulation framework, which may encompass the utilization of simplified material properties or the disregard of specific physical properties which could hold significance in the experimental PSCs.

It is significant that the outcomes of the modeling can offer notable perspectives on the functionality of the cell and direct the enhancement of the device's configuration. The modeling methodology facilitates an organized examination into the impact of multiple variables on the functionality of the device. These variables may include the layer thickness, doping levels, and energy gap. By identifying the optimal configuration that maximizes the PCE, researchers can guide the design and fabrication of more efficient and stable DJ perovskite solar cells.

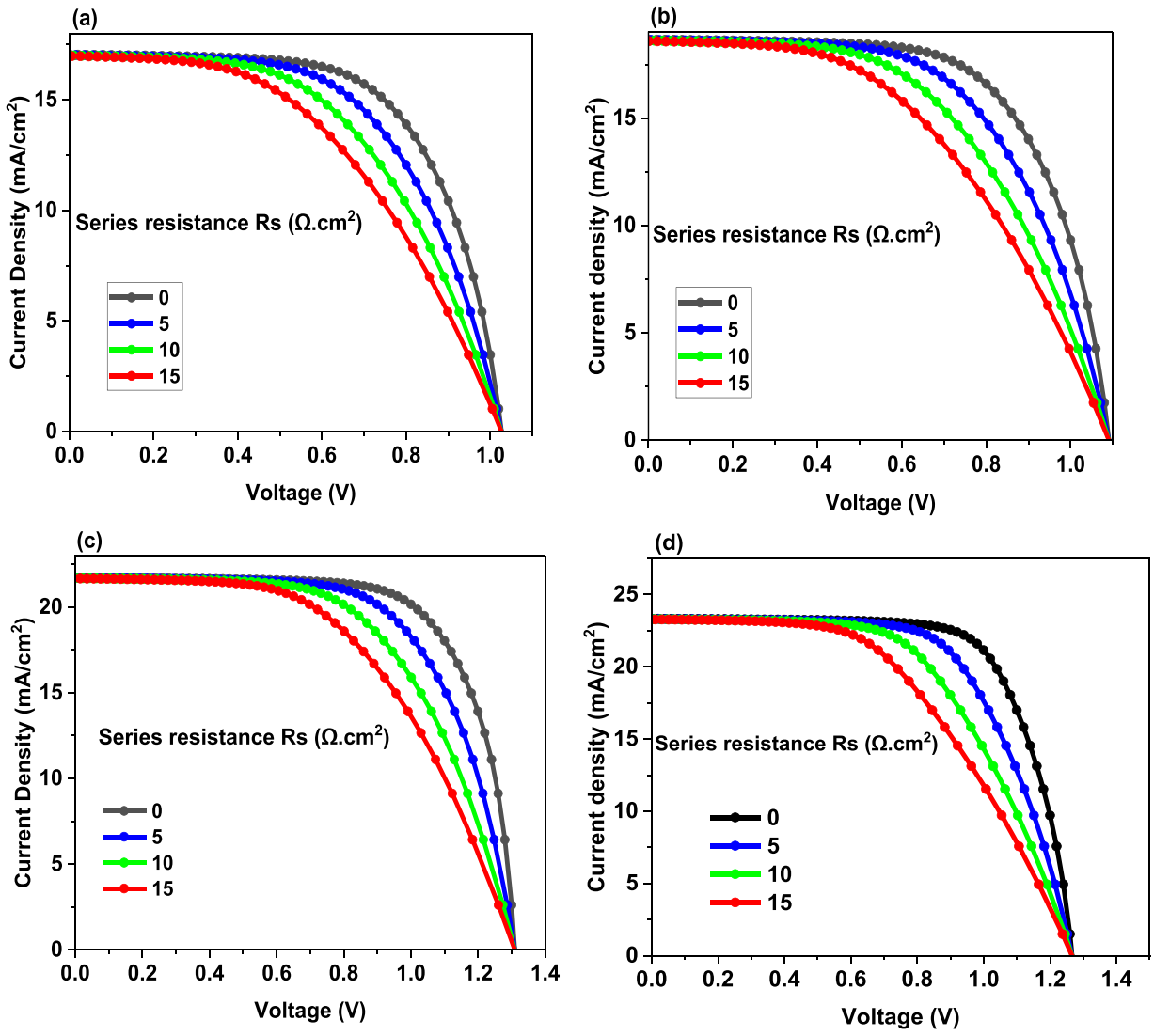

Fig. 4. The influence of R_S on the *J-V* curve of FTO/PCBM/DJ Perovskite/NiO_x/Au PSCs. Where the DJ Perovskite layers are: (a) $n = 3$, (b) $n = 4$, (c) $n = 5$ and (d) $n = 6$.

Table 5
Parameters of FTO/PCBM/DJ Perovskite /NiOx/Au PSCs with different series resistance (R_S) and different layer number (n).

Perovskite	R_S (Ω.cm^2)	V_{oc} (V)	J_{sc} (mA/cm^2)	FF (%)	PCE (%)
$PeDAMA_2Pb_3I_{10}$	0	1.027056	17.04584	64.159	11.2323
	5	1.027132	17.02887	58.1562	10.172
	10	1.027166	17.00738	52.5633	9.1825
	15	1.027185	16.97921	47.4526	8.2761
$PeDAMA_3Pb_4I_{13}$	0	1.091345	18.65395	65.2884	13.2913
	5	1.091435	18.63728	58.9766	11.9967
	10	1.091475	18.61606	53.0937	10.7881
	15	1.091499	18.58803	47.7239	9.6826
$PeDAMA_4Pb_5I_{16}$	0	1.31019	21.71724	71.2608	20.2763
	5	1.310465	21.70499	64.6945	18.4015
	10	1.310563	21.68967	58.476	16.6222
	15	1.310612	21.67007	52.6867	14.9636
$PeDAMA_5Pb_6I_{19}$	0	1.266841	23.32806	71.6565	21.1766
	5	1.267006	23.31583	64.0209	18.9126
	10	1.267066	23.3004	56.7351	16.75
	15	1.267096	23.28019	49.9667	14.7393

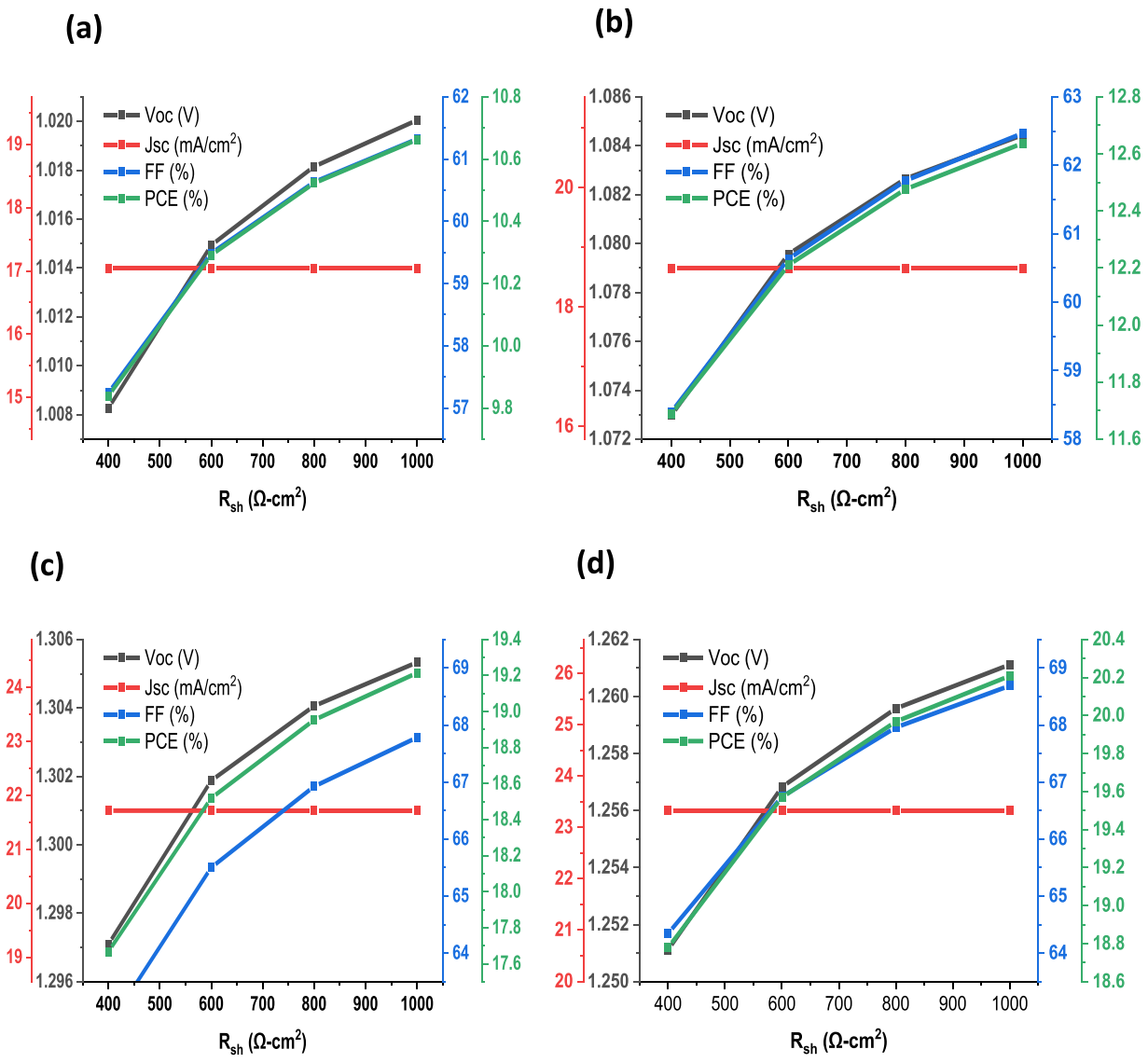

Fig. 5. The influence of R_{sh} on the device parameters of FTO/PCBM/DJ Perovskite/NiO_x/Au PSCs. Where the DJ Perovskite layers are: (a) $n = 3$, (b) $n = 4$, (c) $n = 5$ and (d) $n = 6$.

4.3. Effect of the series and shunt resistance (R_s & R_{sh})

In solar cells, the series resistance (R_S) and shunt resistance (R_{sh}) play a critical role in determining device performance. They originate from the metal contacts that connect the solar cell and the layers that make it up [39]. To examine the impact of R_s on device efficiency, the researchers varied its value from 0 to 15 Ω.cm^2. Fig. 4a-d depict the changes in the *J-V* curve for different numbers of DJ perovskite layers (n) resulting from the changes in R_s.

Interestingly, as the number of DJ perovskite layers increased, the impact of series resistance became more significant. The V_{OC} and J_{SC} were not significantly affected by changes in R_S. However, changes in the FF were substantial, as shown in Table 5. These results suggest that controlling the resistance within a solar cell is crucial for achieving optimal device efficiency.

Inefficient shunt resistance can lead to a higher degree of power loss in solar cells, as it allows the current generated by sunlight to find an alternate path. This undesirable diversion reduces the voltage output of the solar cells and limits the photo-generated current to flow across the cell. As exhibited in Fig. 5a-d, the most significant impact is observed in the FF, which ultimately results in a decline in the PCE value. On the other hand, the V_{OC} and the J_{SC} remain relatively stable and unchanged despite the presence of poor shunt resistance because J_{SC} is determined by the external illumination and the intrinsic properties of the PSC. The R_{sh}, on the other hand, affects the internal behavior of the PSC and the way it handles the flow of current. When the shunt resistance is reduced, the internal resistance of the device is decreased, and more current flows through the shunt path, bypassing the load [40,41]. Consequently, it is crucial to address and improve shunt resistance to optimize solar cell performance and minimize power loss.

Table 6 and Fig. 6 illustrate that the performance of various DJ perovskite cells varies with temperature. Interestingly, some cells display a decline in performance as the temperature increases, while others exhibit an improvement in performance. $PeDAMA_2Pb_3I_{10}$ and $PeDAMA_3Pb_4I_{13}$ exhibit a decrease in J_{SC}, FF, and PCE with increasing temperature due to the decrease in the absorption coefficient of the perovskite material and the increase in recombination losses at higher temperatures. In contrast, $PeDAMA_4Pb_5I_{16}$ and $PeDAMA_5Pb_6I_{19}$ exhibit an increase in J_{SC} and PCE with increasing temperature due to the increase in charge carrier mobility with increasing temperature, which enhances the collection of photo-generated charge carriers. However, the decrease in V_{OC} observed in $PeDAMA_4Pb_5I_{16}$ and $PeDAMA_5Pb_6I_{19}$ is

Table 6
Parameters of FTO/PCBM/DJ Perovskite /NiOx/Au devices under different operational temperatures for various DJ perovskite layers.

Perovskite	Temperature (K)	V_{OC} (V)	J_{SC} (mA/cm^2)	FF (%)	PCE (%)
$PeDAMA_2Pb_3I_{10}$	293	1.03	17.05	64.46	11.29
	303	1.03	17.05	64.04	11.21
	313	1.03	17.05	63.63	11.13
	323	1.02	17.05	63.25	11.05
	333	1.02	17.05	62.88	10.97
$PeDAMA_3Pb_4I_{13}$	293	1.09	18.65	65.59	13.36
	303	1.09	18.65	65.16	13.26
	313	1.09	18.65	64.76	13.17
	323	1.09	18.65	64.37	13.08
	333	1.09	18.65	63.99	12.99
$PeDAMA_4Pb_5I_{16}$	293	1.32	21.72	71.20	20.37
	303	1.31	21.72	71.29	20.24
	313	1.30	21.72	71.44	20.11
	323	1.28	21.72	71.64	19.98
	333	1.27	21.72	71.89	19.85
$PeDAMA_5Pb_6I_{19}$	293	1.27	23.32	71.71	21.35
	303	1.26	23.32	71.62	21.09
	313	1.24	23.32	71.54	20.83
	323	1.23	23.32	71.47	20.56
	333	1.21	23.33	71.39	20.30

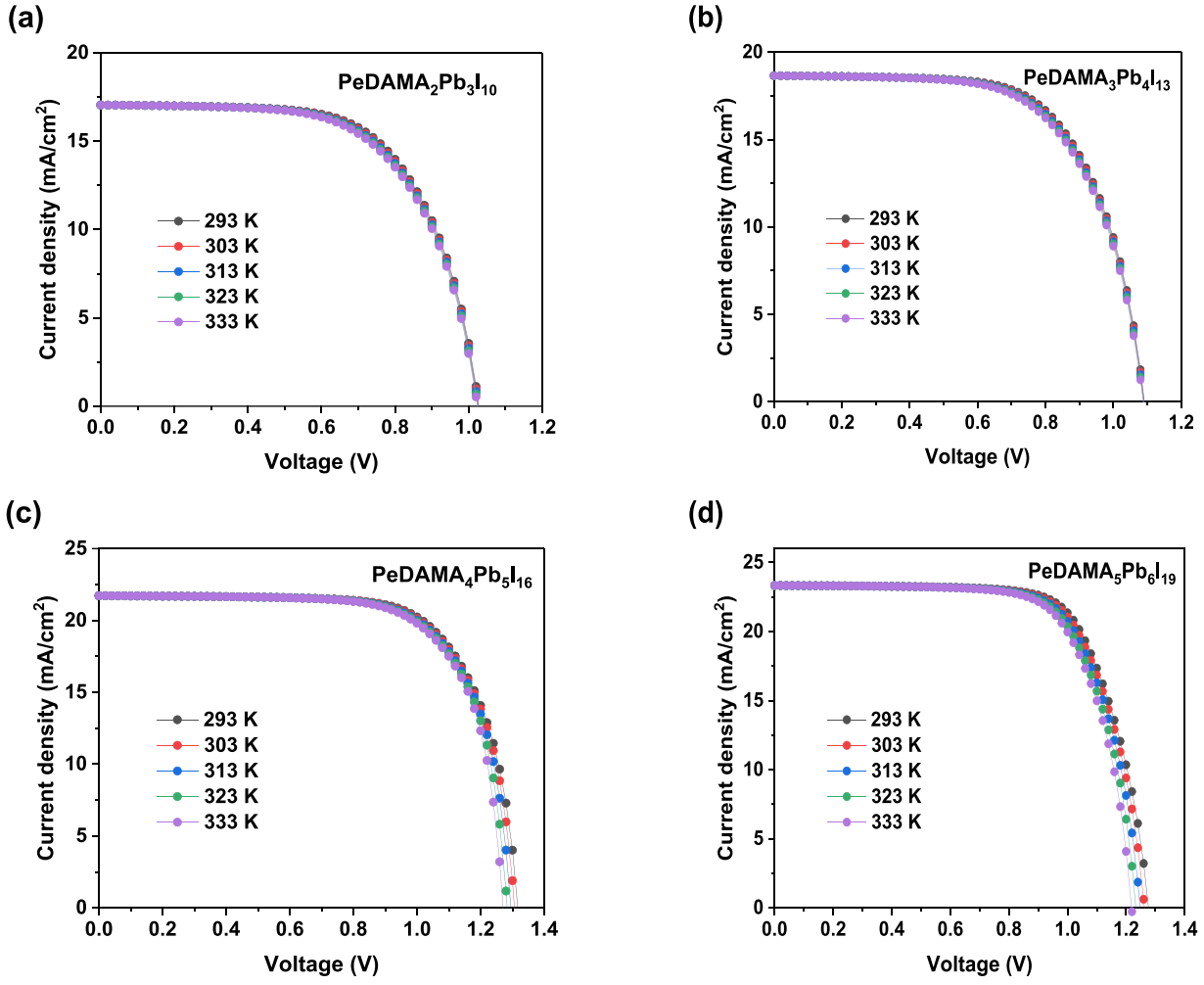

Fig. 6. The influence of operational temperature on the *J-V* curve of FTO/PCBM/DJ Perovskite/NiO_x/Au PSCs. Where the DJ Perovskite layers are: (a) $n = 3$, (b) $n = 4$, (c) $n = 5$ and (d) $n = 6$.

due to the increase in charge carrier recombination at higher temperatures. Additionally, $PeDAMA_5Pb_6I_{19}$ exhibits a decrease in FF due to the increase in non-radiative recombination losses at higher temperatures.

5. Conclusions

The DJ perovskite solar cells, with the structure FTO/PCBM/2D-Perovskite/NiO_x/Au of different layer numbers (n), have different impacts on the solar cell parameters. These variations on the PCE values are based on differences in physical properties such as the electron affinity and the energy gap. Although the stability of the PCS is much higher when the number of layers is small (from the literature), the best efficiency is found at a higher number of layers (in this paper, $n = 6$). The thickness of the DJ perovskite has been observed to influence the performance of the solar cell; the FF has the maximum value at $n = 3$, while the J_{SC} has the lowest value compared to its value at other thicknesses, with the best result found at 0.6 μm. The analysis of the series and shunt resistances emphasizes that an efficient DJ perovskite solar cell requires high shunt resistance (to minimize leakage currents) and low series resistance (to minimize resistive losses). Proper material selection, device architecture, and fabrication techniques are critical to achieving optimal resistance values and, consequently, high-performance perovskite solar cells. Based on our research findings, it appears that the proposed device structure incorporating DJ perovskite may effectively address the stability issues commonly found in 3D perovskite solar cells. Moreover, DJ perovskite-based solar cells demonstrate suitable efficiency, indicating their potential as a viable alternative in future studies.

CRediT authorship contribution statement

Ali K. Al-Mousoi: Conceptualization, Formal analysis, Methodology, Writing – original draft, Writing – review & editing **Burragoni Sravanthi Goud:** Conceptualization, Formal analysis, Methodology, Writing – original draft, Writing – review & editing. **Mustafa K. A. Mohammed**: Conceptualization, Formal analysis, Methodology, Writing – original draft, Writing – review & editing. **Anjan Kumar**: Conceptualization, Formal analysis, Methodology, Writing – original draft, Writing – review & editing **Michael M. Sabugaa**: Conceptualization, Formal analysis, Methodology, Writing – original draft, Writing – review & editing **Ramanjaneyulu Seemaladinne:** Supervision, Writing – review & editing. **Rahul Pandey:** Conceptualization, Formal analysis, Methodology, Writing – original draft, Writing – review & editing. **Jaya Madan**: Conceptualization, Formal analysis, Methodology, Writing – original draft, Writing – review & editing. **M. Khalid Hossain**: Investigation, Validation. **Abdullah A. Al-Kahtani**: Funding acquisition.

Declaration of Competing Interest

The authors declare that they have no known competing financial interests or personal relationships that could have appeared to influence the work reported in this paper.

Data availability

Data will be made available on request.

Acknowledgements

The authors are grateful to the Researchers Supporting Project number (RSP2023R266), King Saud University, Riyadh, Saudi Arabia for the financial support.

References

[1] Y. Ye, Y. Yin, Y. Chen, S. Li, L. Li, Y. Yamauchi, Metal-organic framework materials in perovskite solar cells: recent advancements and perspectives, Small (2023), 2208119.
[2] L. Xu, W. Qiu, M. Feng, Z. Liang, W. Qian, C. Zhou, D. Zhang, M. Li, W. Lv, Y. Tao, Multifunctional resonance bridge-mediated dynamic modulation of perovskite films for enhanced intrinsic stability of photovoltaics, Small (2023), 2207226.
[3] L. Yang, H. Zhou, Y. Duan, M. Wu, K. He, Y. Li, D. Xu, H. Zou, S. Yang, Z. Fang, 25.24%-efficiency FACsPbI3 perovskite solar cells enabled by intermolecular esterification reaction of DL-carnitine hydrochloride, Adv. Mater. (2023), 2211545.
[4] Y. Che, Z. Liu, Y. Duan, J. Wang, S. Yang, D. Xu, W. Xiang, T. Wang, N. Yuan, J. Ding, Hydrazide derivatives for defect passivation in pure CsPbI3 perovskite solar cells, Angew. Chem. Int. Ed. 61 (33) (2022), e202205012.
[5] S.M. Majeed, M.K. Mohammed, D.S. Ahmed, Efficient and hysteresis-free mixed-dimensional 2D/3D perovskite solar cells using ethyl lactate as a green additive to perovskite precursor solutions, J. Mater. Chem. C. 10 (43) (2022) 16480–16491.
[6] G.-H. Kim, D.S. Kim, Development of perovskite solar cells with> 25% conversion efficiency, Joule 5 (5) (2021) 1033–1035.
[7] H. Min, D.Y. Lee, J. Kim, G. Kim, K.S. Lee, J. Kim, M.J. Paik, Y.K. Kim, K.S. Kim, M. G. Kim, Perovskite solar cells with atomically coherent interlayers on SnO2 electrodes, Nature 598 (7881) (2021) 444–450.
[8] J. Jeong, M. Kim, J. Seo, H. Lu, P. Ahlawat, A. Mishra, Y. Yang, M.A. Hope, F. T. Eickemeyer, M. Kim, Pseudo-halide anion engineering for α-FAPbI3 perovskite solar cells, Nature 592 (7854) (2021) 381–385.
[9] A. Kojima, K. Teshima, Y. Shirai, T. Miyasaka, Organometal halide perovskites as visible-light sensitizers for photovoltaic cells, J. Am. Chem. Soc. 131 (17) (2009) 6050–6051.
[10] S. Khatoon, V. Chakraborty, S.K. Yadav, S. Diwakar, J. Singh, R.B. Singh, Simulation study of CsPbIxBr1-x and MAPbI3 heterojunction solar cell using SCAPS-1D, Sol. Energy 254 (2023) 137–157.
[11] X. Chu, Q. Ye, Z. Wang, C. Zhang, F. Ma, Z. Qu, Y. Zhao, Z. Yin, H.-X. Deng, X. Zhang, Surface in situ reconstruction of inorganic perovskite films enabling long carrier lifetimes and solar cells with 21% efficiency, Nature, Energy (2023) 1–9.
[12] Y. Xiong, M. Li, L. Peng, A.A. Thant, N. Wang, Y. Zhu, L. Xu, Highly Efficient and Stable 2D/3D Heterojunction Perovskite Solar Cells by In Situ Interface Modification with [(p-Fluorophenyl) ethyl] ammonium Acetate, ACS Applied Materials & Interfaces (2023).
[13] M.S. Mehde, A.M. Al-Gebori, A.K. Hantoosh, The effect of the spinning speed variation on the perovskite solar cell efficiency, IOP Conference Series: Materials Science and Engineering, IOP Publishing, 2020, p. 012071.
[14] M.K. Mohammed, M.S. Jabir, H.G. Abdulzahraa, S.H. Mohammed, W.K. Al-Azzawi, D.S. Ahmed, S. Singh, A. Kumar, S. Asaithambi, M. Shekargoftar, Introduction of cadmium chloride additive to improve the performance and stability of perovskite solar cells, RSC Adv. 12 (32) (2022) 20461–20470.
[15] M.K. Mohammed, R.K. Al-Azzawi, H.H. Jasim, S.H. Mohammed, S. Singh, H. H. Kadhum, A. Kumar, P. Sasikumar, M. Revathy, M.S. Jabir, Adaption of MAPbI3 perovskite with copper phthalocyanine inorganic hole transport layer via nitrosonium tetrafluoroborate additive to enhance performance and stability of perovskite solar cells, Opt. Mater. 133 (2022), 112901.
[16] Y. Zheng, T. Niu, J. Qiu, L. Chao, B. Li, Y. Yang, Q. Li, C. Lin, X. Gao, C. Zhang, Oriented and uniform distribution of Dion–Jacobson phase perovskites controlled by quantum well barrier thickness, Sol. Rrl 3 (9) (2019), 1900090.
[17] J. Xiang, X. Li, S. Gong, S. Wang, X. Chen, F. Zhang, Green-antisolvent-induced homogeneous phase distribution for efficient and stable MA-free 2D perovskite solar cells, Chem. Eng. J. 460 (2023), 141758.
[18] X. Guo, Y. Gao, F. Long, L. Lin, Y. Wang, K.H. Ngai, Q. Wei, G. Xing, T. Shi, W. Xie, The interplay of organic spacer and small cation for efficient Dion-Jacobson perovskite solar cells, Solar RRL.
[19] C.C. Stoumpos, D.H. Cao, D.J. Clark, J. Young, J.M. Rondinelli, J.I. Jang, J. T. Hupp, M.G. Kanatzidis, Ruddlesden–Popper hybrid lead iodide perovskite 2D homologous semiconductors, Chem. Mater. 28 (8) (2016) 2852–2867.
[20] Y. Dong, X. Dong, D. Lu, M. Chen, N. Zheng, R. Wang, Q. Li, Z. Xie, Y. Liu, Orbital interactions between the organic semiconductor spacer and the inorganic layer in dion–jacobson perovskites enable efficient solar cells, Adv. Mater. 35 (3) (2023), 2205258.
[21] B. Zhou, D. Yan, Simultaneous long-persistent blue luminescence and high quantum yield within 2D organic–metal halide perovskite micro/nanosheets, Angew. Chem. 131 (42) (2019) 15272–15279.
[22] J.-C. Blancon, J. Even, C.C. Stoumpos, M.G. Kanatzidis, A.D. Mohite, Semiconductor physics of organic–inorganic 2D halide perovskites, Nat. Nanotechnol. 15 (12) (2020) 969–985.
[23] X. Han, Y. Zheng, S. Chai, S. Chen, J. Xu, 2D organic-inorganic hybrid perovskite materials for nonlinear optics, Nanophotonics 9 (7) (2020) 1787–1810.
[24] J. Chen, B. Wang, G. Huang, Q. Cheng, Y. Li, X. Li, S. Li, K. Li, L. Zhu, Z. Zhai, Thermally regulated energy loss in dion–jacobson perovskite solar cells, Sol. RRL 6 (11) (2022), 2200636.
[25] M. Burgelman, P. Nollet, S. Degrave, Modelling polycrystalline semiconductor solar cells, Thin Solid films 361 (2000) 527–532.
[26] S. Karthick, S. Velumani, J. Bouclé, Experimental and SCAPS simulated formamidinium perovskite solar cells: a comparison of device performance, Sol. Energy 205 (2020) 349–357.
[27] A. Kumar, S. Singh, M.K. Mohammed, A.E. Shalan, Computational modelling of two terminal CIGS/perovskite tandem solar cells with power conversion efficiency of 23.1%, Eur. J. Inorg. Chem. 2021 (47) (2021) 4959–4969.

[28] A.K. Al-Mousoi, M.K. Mohammed, R. Pandey, J. Madan, D. Dastan, G. Ravi, P. Sakthivel, Simulation and analysis of lead-free perovskite solar cells incorporating cerium oxide as electron transporting layer, RSC Adv. 12 (50) (2022) 32365–32373.
[29] M.K. Hossain, A. Arnab, R.C. Das, K. Hossain, M. Rubel, M.F. Rahman, H. Bencherif, M. Emetere, M.K. Mohammed, R. Pandey, Combined DFT, SCAPS-1D, and wxAMPS frameworks for design optimization of efficient Cs 2 BiAgI 6-based perovskite solar cells with different charge transport layers, RSC Adv. 12 (54) (2022) 35002–35025.
[30] A.K. Al-Mousoi, M.K. Mohammed, S.Q. Salih, R. Pandey, J. Madan, D. Dastan, E. Akman, A.A. Alsewari, Z.M. Yaseen, Comparative study of the correlation between diffusion length of charge carriers and the performance of CSSNGEI3 perovskite solar cells, Energy Fuels 36 (23) (2022) 14403–14410.
[31] A. Kumar, S. Singh, M.K. Mohammed, Numerical investigation of single junction environmental friendly double perovskite (Cs2AuBiCl6) solar cell with 20.5% power conversion efficiency and negligible hysteresis, Int. J. Energy Res. 46 (14) (2022) 20180–20193.
[32] S.S. Hussain, S. Riaz, G.A. Nowsherwan, K. Jahangir, A. Raza, M.J. Iqbal, I. Sadiq, S.M. Hussain, S. Naseem, Numerical modeling and optimization of lead-free hybrid double perovskite solar cell by using SCAPS-1D, J. Renew. Energy 2021 (2021) 1–12.
[33] T. Dureja, A. Garg, S. Bhalla, D. Bhutani, A. Khanna, Double lead-free perovskite solar cell for 19.9% conversion efficiency: A SCAPS-1D based simulation study, Mater. Today.: Proc. 71 (2022) 239–242.
[34] A. Thakur, D. Singh, S.K. Gill, Numerical simulations of 26.11% efficient planar CH3NH3PbI3 perovskite nip solar cell, Mater. Today.: Proc. 71 (2022) 195–201.
[35] J.-M. Hwang, D. Schroder, Recombination properties of oxygen-precipitated silicon, J. Appl. Phys. 59 (7) (1986) 2476–2487.
[36] J. Chakrabartty, M.A. Islam, S. Reza, Performance analysis of highly efficient 2D/3D bilayer inverted perovskite solar cells, Sol. Energy 230 (2021) 195–207.
[37] D. Pal, A. Comprehensive, Analysis of eco-friendly Cs2SnI6 based tin halide perovskite solar cell through device modeling, Adv. Theory Simul. 6 (3) (2023), 2200856.
[38] G. Huang, J. Chen, B. Wang, Q. Cheng, Y. Li, Su Zafar, T. Yue, Y. Yan, W. Du, H. Zhang, Solvent effect on film formation and trap states of two-dimensional dion–jacobson perovskite, Nano Lett. 22 (18) (2022) 7545–7553.
[39] Z. Bi, S. Zhang, M. Thandapani, Y. Zhu, Y. Zheng, N.Q. Liem, X. Xiao, G. Xu, A. Guerrero, X. Xu, High shunt resistance SNO2–Pbo electron transport layer for perovskite solar cells used in low lighting applications, Adv. Sustain. Syst. 5 (11) (2021), 2100120.
[40] M.K. Hossain, G.I. Toki, J. Madan, R. Pandey, H. Bencherif, M.K. Mohammed, M. R. Islam, M. Rubel, M.F. Rahman, S. Bhattarai, A comprehensive study of the optimization and comparison of cesium halide perovskite solar cells using ZnO and Cu2FeSnS4 as charge transport layers, N. J. Chem. 47 (2023) 8602–8624.
[41] M.K. Hossain, M.K. Mohammed, R. Pandey, A. Arnab, M. Rubel, K. Hossain, M. H. Ali, M.F. Rahman, H. Bencherif, J. Madan, Numerical analysis in DFT and SCAPS-1D on the influence of different charge transport layers of CsPbBr3 Perovskite solar cells, Energy Fuels 37 (2023) 6078–6098.